*Cerebral Cortex*, July 2021;31: 3213–3225

**doi: 10.1093/cercor/bhab001**
Advance Access Publication Date: 27 February 2021
Original Article

ORIGINAL ARTICLE

# A Structure–Function Substrate of Memory for Spatial Configurations in Medial and Lateral Temporal Cortices

Shahin Tavakol[1], Qiongling Li[1], Jessica Royer[1], Reinder Vos de Wael[1], Sara Larivière[1], Alex Lowe[1], Casey Paquola[1], Elizabeth Jefferies[2], Tom Hartley[2], Andrea Bernasconi[1], Neda Bernasconi[1], Jonathan Smallwood[2], Veronique Bohbot[3], Lorenzo Caciagli[4,5,†] and Boris Bernhardt[1,†]

[1]McConnell Brain Imaging Centre, Montreal Neurological Institute and Hospital, McGill University, Montreal, Quebec H3A 2B4, Canada, [2]University of York, York YO10 5DD, UK, [3]Douglas Mental Health University Institute, McGill University, Montreal, Quebec H4H 1R3, Canada, [4]Department of Clinical and Experimental Epilepsy, UCL Queen Square Institute of Neurology, WC1N 3BG London, United Kingdom and [5]Department of Bioengineering, University of Pennsylvania, Philadelphia, PA 19104, USA

Address correspondence to Boris Bernhardt, PhD, Multimodal Imaging and Connectome Analysis Lab, McConnell Brain Imaging Centre, Montreal Neurological Institute and Hospital, McGill University, Montreal, Quebec, Canada. Email: boris.bernhardt@mcgill.ca.

[†]Lorenzo Caciagli and Boris Bernhardt are joint co-authors.



## Abstract

Prior research has shown a role of the medial temporal lobe, particularly the hippocampal–parahippocampal complex, in spatial cognition. Here, we developed a new paradigm, the conformational shift spatial task (CSST), which examines the ability to encode and retrieve spatial relations between unrelated items. This task is short, uses symbolic cues, incorporates two difficulty levels, and can be administered inside the scanner. A cohort of 48 healthy young adults underwent the CSST, together with a set of behavioral measures and multimodal magnetic resonance imaging (MRI). Inter-individual differences in CSST performance correlated with scores on an established spatial memory paradigm, but neither with episodic memory nor mnemonic discrimination, supporting specificity. Analyzing high-resolution structural MRI data, individuals with better spatial memory showed thicker medial and lateral temporal cortices. Functional relevance of these findings was supported by task-based functional MRI analysis in the same participants and ad hoc meta-analysis. Exploratory resting-state functional MRI analyses centered on clusters of morphological effects revealed additional modulation of intrinsic network integration, particularly between lateral and medial temporal structures. Our work presents a novel spatial memory paradigm and supports an integrated structure–function substrate in the human temporal lobe. Task paradigms are programmed in python and made open access.

**Key words:** spatial memory, neuroimaging, task fMRI, medial temporal lobe

## Introduction

Spatial memory is characterized by the encoding and retrieval of spatial associations. In rodents, structures of the medial temporal lobe (MTL) have long been recognized as crucial neural substrates of spatial memory (O'Keefe and Dostrovsky 1971; O'Keefe and Nadel 1978; Winocur 1982; Morris et al. 1982; Aggleton et al. 1986; Hafting et al. 2005). In humans, early studies in patients with temporal lobe epilepsy revealed a direct correlation between the severity of MTL lesions and deficits in spatial cognition (Milner 1965; Smith and Milner 1981; Smith and Milner 1989; Rains and Milner 1994). Ensuing neuroimaging and lesion experiments in neurological patients reinforced the significance of the MTL as a critical brain structure in spatial memory processing, but also pointed to an involvement of other brain regions and the broader conceptualization of spatial memory as a network phenomenon (Aguirre et al. 1996; Ghaem et al. 1997; Maguire et al. 1998). The role of the MTL as a spatial processing hub was further supported by the discovery of human place cells and grid cells, specialized neurons believed to instantiate a scalable and navigable mental representation of space (Ekstrom et al. 2003; Jacobs et al. 2013).

The structural organization of spatial memory relies on the interplay between brain morphology and relevant cognitive phenotypes. For instance, the association between the volume of the MTL and behavioral measures of spatial cognition has been reported since the earliest structural magnetic resonance imaging (sMRI) studies (Abrahams et al. 1999; Maguire et al. 2000; Hartley and Harlow 2012). Today, state-of-the-art automated segmentation tools can generate surface-wide representations of the brain, sampling morphological markers such as neocortical thickness and volume of hippocampal subregions with unprecedented resolution (Bernhardt et al. 2016; Kim et al. 2014; Kim et al. 2005; Fischl 2012; Wang et al. 2013; Caldairou et al. 2016; Romero et al. 2017; Goubran et al. 2020). These millimetric anatomical indices are ideal for investigating the link between morphological and behavioral variability across individuals. Complementing sMRI studies, a large body of research has focused on the analysis of functional MRI (fMRI) acquisitions. Task-based fMRI studies have shown consistent MTL involvement during spatial memory tasks, together with activations in neocortical areas (Aguirre and D'Esposito 1997; Jokeit et al. 2001; Hassabis et al. 2009; Schindler and Bartels 2013). Complementing these paradigms, resting-state fMRI (rs-fMRI) enables to interrogate intrinsic functional networks (Biswal et al. 1997; Buckner et al. 2013; Cordes et al. 2000; Lowe et al. 2000; Fox et al. 2006; Smith et al. 2009). An increasing body of rs-fMRI studies has also assessed intrinsic functional network substrates underlying interindividual differences in cognitive capacities (Smith et al. 2015; Medea et al. 2018; Sormaz et al. 2017; He et al. 2020).

The current study devised a new and open-access paradigm to assess spatial memory in humans and to elucidate the functional anatomy of spatial memory processing via structural and functional MRI analyses. We developed the conformational shift spatial task (CSST), a short, easy-to-use assessement that taps into the capacity to encode and retrieve spatial interdependencies between three conceptually unrelated objects. We administered the CSST to 48 healthy indivuals inside a 3 T Siemens Magnetom Prisma scanner as part of a broader task-based fMRI battery, which included additional testing probes for semantic memory, episodic memory, and mnemonic discrimination. Together with the semantic and episodic memory tasks, the CSST constitutes an integral part of a relational memory fMRI battery that can address structural and functional convergence and divergence across relational mnemonic domains. All three tests were homogenized by (i) implementing comparable visual stimuli, (ii) incorporating task difficulty modulation across two conditions (i.e., 28 easy trials and 28 difficult trials), (iii) using a three-alternative forced choice trial-by-trial paradigm. Given that these tasks are designed to probe different domains of relational memory, we hypothesized that behavioral scores on the CSST would correlate with performances on the semantic and episodic association tasks, with greater association observed between spatial and semantic domains (Nadel and Moscovitch 1997; Moscovitch et al. 2005; McNaughton et al. 2006; Constantinescu et al. 2016; Bellmund et al. 2018; Mok and Love 2019). We also evaluated participants with supplementary assessment tools outside the scanner, including the four mountains task (FMT), an established spatial memory paradigm that uses scenes rather than symbolic stimuli, and which does not have varying difficulty levels (Hartley et al. 2007). We further hypothesized that CSST performance would show strongest correlations with performance on the FMT, as both tasks are devised to assess the same relational domain, that is, spatial processing. In addition to its task-based section, our protocol encompassed structural MRI as well as rs-fMRI acquisitions. We used these to assess associations between spatial memory scores and variations in MRI-derived morphological measures of cortical thickness and hippocampal volume across participants. Although surface-based analyses were regionally unconstrained, based on prior literature in humans and animals studying spatial memory (O'Keefe and Nadel 1978; Morris et al. 1982; Smith and Milner 1989; Rains and Milner 1994; Aguirre and D'Esposito 1997; Abrahams et al. 1999; Maguire et al. 2000; Jokeit et al. 2001; Hafting et al. 2005; Hassabis et al. 2009; Hartley and Harlow 2012; Schindler and Bartels 2013), we expected to observe structure–function substrates in the medial temporal lobe regions, such as the parahippocampal gyrus. Results were contextualized against task-based fMRI findings in the same participants and ad hoc meta-analytical inference. Structural imaging observations were further used for post hoc explorations of rs-fMRI connectivity modulations by interindividual differnces in task performance.

## METHODS

### Participants

A total of 48 healthy adults (16 women, mean age $\pm$ SD = 29.71 $\pm$ 6.55 years, range: 19 to 44 years, four left-handed), recruited in 2018 and 2019, participated in our study and had normal or corrected-to-normal vision. Control participants did not have any neurological or psychiatric diagnosis. Our study was approved by the Research Ethics Committee of the McGill University and participants gave written and informed consent upon arrival at the Montreal Neurological Institute.

### Conformational Shift Spatial Task

In the CSST, the participant discriminated the spatial arrangement of three semantically unrelated items (i.e., a brick, a tire, a bucket) from two additional foil configurations of the same items (Fig. 1*a*). At each trial, following a jittered inter-trial interval (1.5–2.5 s), the participant encoded the salient features of an original trio arrangement for a duration of 4 s. Following a jittered inter-stimulus interval (0.5–1.5 s), three distinct versions

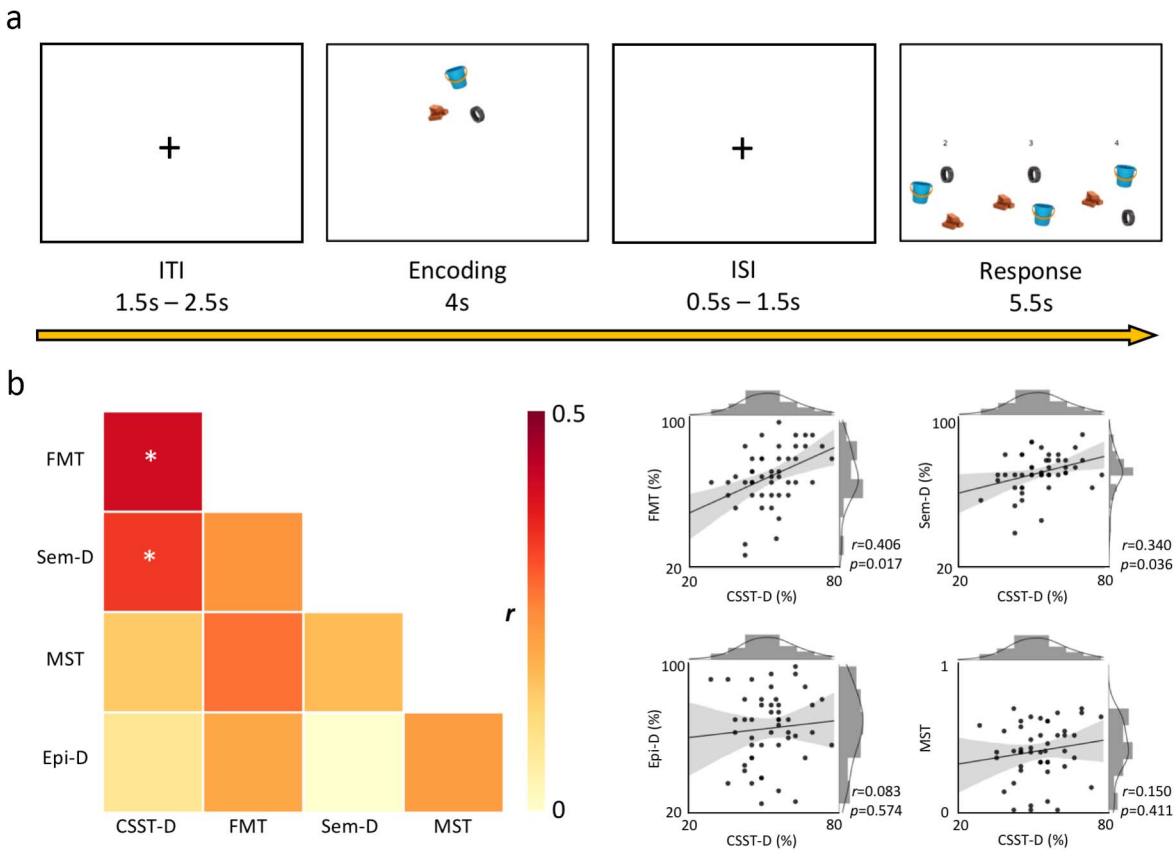


Figure 1. Task design and behavioral associations. (*a*) Following a jittered inter-trial interval (ITI), the participant had to encode the spatial configuration of the stimulus trio for 4 s. After a jittered inter-stimulus interval (ISI), the participant had 5.5 s to choose the original spatial conformation among two foil options. (*b*) left panel: correlation heat map of performance across all tasks. CSST-D shows significant associations with FMT and Sem-D following adjustment for false discovery rate ($*p_{FDR} < 0.05$). Right panel: joint-plot of CSST-D associations with other tasks (CSST-D: conformational shift spatial task-difficult, FMT: four mountains task, Sem-D: semantic task-difficult, MST: mnemonic similarity/discrimination task, Epi-D: episodic difficult).

of the trio were displayed. All three conformations had undergone an equal rotation about the trio center of mass between 45° clockwise to 45° counterclockwise. The correct conformation had not undergone any additional transformation unlike the other two foils.

In the "difficult" condition (i.e., CSST-D), the two distractor layouts had been subjected to "one" specific additional transformation each: the spacing between the three items had changed with respect to the original configuration. In the "easy" condition (i.e., CSST-E), the foil configurations had undergone "two" specific additional transformations each: (1) the spacing between the three items had changed with respect to the original configuration; (2) the relative positions of trio items had been swapped. The participant was allowed up to 5.5 s to select the correct response. Thus, distractors in "difficult" trials varied from the original configuration by 2 degrees of separation (i.e., rotation about the center of mass and spacing alteration), whereas distractors in "easy" trials comprised 3 degrees (i.e., rotation about the center of mass, spacing alteration, and item positional swap).

The entire task was composed of 56 pseudo-randomized trials (i.e., 28 easy, 28 difficult). The semantic inter-relatedness of the trio items was computed via the UMBC Phrase Similarity Service (Han et al. 2013). Based on the frequency with which two nouns representing the presented visual symbols co-occur within the Refined Stanford WebBase Corpus, which contains 100 million web pages from over 50 000 websites, this algorithm computed a conceptual relatedness index. We implemented prototypical visual stimuli as proxies for selected lexical entries whose similarity indices were inferior to 0.3 (range: 0–1).

## Additional Cognitive Tasks

*Four Mountains Task (Hartley et al. 2007)*

The FMT is an established spatial cognition paradigm. In this version, 15 trials were administered in total. At each trial, the participant had 10 s to encode the spatially relevant stimuli within a computer-rendered landscape composed of four distinct mountains varying in shape and size. After the encoding phase, participants had to select the correct landscape in a four-alternative-forced-choice paradigm. The correct answer corresponded to the originally encoded landscape albeit depicted from a different first-person perspective, whereas the three incorrect options showed renderings of four mountains with different characteristics and configurations. All choices were additionally modified along lighting, weather, and vegetation texture to control for visual matching strategies. There was no time limit, but participants were instructed to respond as quickly and as accurately as possible. Following each trial, participants had to report how certain they were about their response (i.e., certain or uncertain).

*Semantic Task*

We used a symbolic variant of a previously used lexicon-based semantic association paradigm (Sormaz et al. 2017; Wang et al. 2018). Consisting of 56 pseudo-randomized trials, the task implements a three-alternative-forced-choice paradigm and is modulated for difficulty across conditions with equal number of trials (i.e., 28 difficult: Sem-D; 28 Easy: Sem-E). At each trial, a target object appeared at the top of the monitor (i.e., apple) with three objects below (i.e., desk, banana, kettle). Participants had to select the bottom item that was conceptually the most similar to the target. The semantic relatedness of items was measured via the UMBC similarity index (see above description regarding CSST). In difficult trials, the correct response and the target shared an index greater or equal to 0.7, whereas the foils shared a similarity index between 0.3 and strictly smaller than 0.7 with the target. In easy trials, the indices were greater than or equal to 0.7 between correct response and target, and 0 to strictly smaller than 0.3 between any given foil and target.

*Episodic Task*

We used a symbolic variant of a previously used lexicon-based paradigm (Sormaz et al. 2017; Payne et al. 2012) that involves two phases. In the encoding phase, participants had to memorize pairs of images shown simultaneously. Each pair was corrected for conceptual relatedness using the UMBC similarity algorithm (see above) with an index smaller than 0.3. The encoding phase was modulated for difficulty across conditions: some trials were shown only once throughout the session, whereas others were displayed twice to ensure more stable encoding. Following a 10 min delay, the retrieval phase was administered. At each trial, participants had to identify the object that was originally paired with the target object from the encoding phase in a three-alternative-forced-choice paradigm, similar to the one described in the semantic task. There were 56 pseudo-randomized trials in total with 28 corresponding to pairs of images encoded only once (i.e., Epi-D) and 28 to pairs of images encoded twice (i.e., Epi-E).

*Mnemonic Similarity (Discrimination) Task (Stark et al. 2013)*

The MST assessed the capacity to discriminate between stimuli with overlapping features. It comprised two phases: encoding and recall, administered ~8 min apart. The encoding phase consisted of 64 trials in which the participant had to choose whether the displayed item belonged "indoors" or "outdoors." The recall phase was based on a three-alternative-forced-choice paradigm. At this stage, the participant had to select whether the presented item was an exact duplicate from the encoding phase (i.e., "old"), an inaccurate duplicate (i.e., "similar"), or an altogether novel stimulus (i.e., "new"). This phase consisted of 32 trials per condition for a total of 96 trials.

## MRI Acquisition

MRI data were acquired on a 3 T Siemens Magnetom Prisma-Fit with a 64-channel head coil. Two T1-weighted (T1w) scans with identical parameters were acquired with a 3D-MPRAGE sequence (0.8 mm isotropic voxels, matrix = 320 × 320, 224 sagittal slices, TR = 2300 ms, TE = 3.14 ms, TI = 900 ms, flip angle = 9°, iPAT = 2). Task and resting-state fMRI time series were acquired using a 2D echo planar imaging sequence (3.0 mm isotropic voxels, matrix = 80 × 80, 48 slices oriented to AC-PC-30 degrees, TR = 600 ms, TE = 30 ms, flip angle = 50°, multiband factor = 6). The CSST task was approximately 15 min long and presented via a back-projection system to the participants. During the 7 min-long rs-fMRI scan, participants were instructed to fixate a cross displayed in the center of the screen and to clear their mind.

## Structural MRI Processing

*Generation of Neocortical Surfaces*

To generate models of the cortical surface and to measure cortical thickness, native T1w images were processed using FreeSurfer 6.0 (http://surfer.nmr.mgh.harvard.edu). Previous work has cross-validated FreeSurfer with histological analysis (Rosas et al. 2002; Cardinale et al. 2014) and manual measurements (Kuperberg et al. 2003). Processing steps have been described in detail elsewhere (Dale et al. 1999; Fischl et al. 1999). In short, the pipeline includes brain extraction, tissue segmentation, pial and white matter surface generation, and registration of individual cortical surfaces to the fsaverage template. This aligns cortical thickness measurement locations among participants, while minimizing geometric distortions. Cortical thickness was calculated as the closest distance from the gray/white matter boundary to the gray matter/cerebrospinal fluid boundary at each vertex. Thickness data underwent spatial smoothing using a surface-based diffusion kernel (FWHM = 10 mm). As in prior work (Valk et al. 2017), data underwent manual quality control and potential correction for segmentation inaccuracies.

## Functional MRI Processing

(a) Task-based fMRI data were preprocessed using SPM12 (https://www.fil.ion.ucl.ac.uk/spm/). Steps included image realignment, distortion correction using AP-PA blip pairs, structural and functional co-registration, as well as functional data normalization and spatial smoothing (FWHM = 6 mm). Of the originally acquired fMRI scans, data for four participants were omitted due to artifacts caused by field inhomogeneity. For the remaining participants (n = 44), first-level mass-univariate analyses were performed by modeling all task regressors into the SPM design matrix, which included trial onsets and durations/reaction times for ITIs, encoding phases, ISIs, retrieval phases, and post-retrieval rest periods, in addition to six standard motion parameters as well as a constant term. Regressors were convolved with the built-in SPM canonical hemodynamic response function without temporal nor dispersion derivatives. Following mass-univariate model estimations, first-level contrast maps from weighted comparisons between retrieval and encoding (i.e., when the participant chooses a specific stimulus configuration vs. when the participant is passively encoding the original stimulus conformation) were used to generate a single group-level activation map, which was thresholded ($p_{FWE}$ = 0.05) and mapped onto fsaverage template using FreeSurfer.

(b) The rs-fMRI scans were preprocessed using a combination of FSL, available at https://fsl.fmrib.ox.ac.uk/fsl/fslwiki (Jenkinson et al. 2012), and AFNI, available at https://afni.nimh.nih.gov/afni (Cox 1996), and included removal of the first five volumes from each time series to ensure magnetization equilibrium, distortion correction based on AP-PA blip pairs, reorientation, motion correction, skull stripping, grand mean scaling, and detrending. Prior to connectivity analysis, time series were statistically corrected for effects of head motion, white matter signal, and CSF signal. They were also band-pass filtered to be within 0.01 to 0.1 Hz. All participants had overall low

head motion and mean frame-wise displace. Following rs-fMRI preprocessing in native space, a boundary-based registration technique (Greve and Fischl 2009) mapped the functional time series to each participant's structural scan and subsequently, to the neocortical and hippocampal surface models. Surface-based fMRI data also underwent spatial smoothing (FWHM = 10 mm).

### Statistical Analysis

Analyses were performed using SurfStat for Matlab (MathWorks, R2019b) available at http://math.mcgill.ca/keith/surfstat (Worsley et al. 2009).

*(A) Behavioral Task Correlation*

To assess the sensitivity and specificity of the newly developed protocol for spatial cognition, we cross-correlated the CSST-D with the FMT, Sem-D, Epi-D, and MST. Given that all participants were high functioning healthy individuals, we only incorporated performance scores on the difficult conditions where applicable, which additionally precluded ceiling effects.

*(B) Cortical Thickness Analysis*

Surface-wide linear models evaluated associations between task scores and cortical thickness:

$$T_i = \beta_0 + \beta_1 * Age + \beta_2 * Sex + \beta_3 * Score + \varepsilon$$

where $T_i$ is the thickness measure at vertex $i$ for a total of 327 684 vertices. "Age," "Sex," and "Score" are model terms, $\beta_0$, $\beta_1$, $\beta_2$, and $\beta_3$, the estimated model parameters, and $\varepsilon$ is the error coefficient.

We then regressed out the effects of Age and Sex from cortical thickness measures:

$$T_i = \beta_0 + \beta_1 * Age + \beta_2 * Sex + \varepsilon \quad rT_i = T_i - (\beta_0 + \beta_1 * Age + \beta_2 * Sex)$$

where $rT_i$ is the residual thickness measure at vertex $i$, corrected for "Age" and "Sex." To assess whether the brain-behavioral correlations were generalizable to another spatial task, we correlated residual thickness from clusters of findings with FMT scores obtained outside the scanner.

*(C) Hippocampal Analysis*

A multi-template surface-patch algorithm was implemented to segment the hippocampus into its subfields (Caldairou et al. 2016; Bernhardt et al. 2016; Styner et al. 2006; Kim et al. 2014 see Supplementary Methods). The product of voxel volume and number of inclusive voxels was computed for each subfield. Next, total hippocampal volume was measured as the sum of all subregional volumes. Volume-based models were then used to assess effects of task scores on the whole hippocampus:

$$V = \beta_0 + \beta_1 * Age + \beta_2 * Sex + \beta_3 * Score + \varepsilon$$

where $V$ is the total volume of the hippocampus. A similar model was run for vertex-wise hippocampal columnar data derived from subfield surface mapping (see Supplementary Methods).

*(D) Functional Contextualization*

Task-based second-level functional activation maps were obtained from 44 participants and thresholded ($p_{FWE} = 0.05$) before being mapped to fsaverage. Average residual (i.e., age- and sex-corrected) cortical thickness across all vertices within regions of activation was then correlated with task scores. Furthermore, Neurosynth-based meta-analysis was used to perform a search for the term "navigation," which resulted in 77 studies with a total of 3908 activations. The generated association map was thresholded ($p_{FDR} = 0.01$) and mapped onto fsaverage. Once more, average residual thickness was computed and correlated with task results.

*(E) Resting-State Connectivity Analysis*

Surface-wide linear models assessed the modulatory effect of task performance on rs-fMRI connectivity between clusters of structural imaging findings *(see B)* and resting-state data:

$$Z_i = \beta_0 + \beta_1 * Age + \beta_2 * Sex + \beta_3 * Score + \varepsilon$$

where $Z_i$ is the Fisher Z-transformed correlation coefficient between mean resting-state intensity for a given cluster in *(B)* and whole brain data at vertex $i$.

We performed a similar analysis to *(j)* to evaluate the effect of task score on functional connectivity between clusters in *(B)* and resting-state data mapped on the hippocampal template.

*(F) Correction for Multiple Comparisons*

We used random field theory for non-isotropic images to correct for multiple comparisons ($p_{FWE} = 0.05$). Main structural MRI findings were based on a stringent cluster-defining threshold of $P = 0.001$. For more exploratory rs-fMRI connectivity analyses, we used a more liberal cluster-defining threshold of $P = 0.025$.

## Results

### Behavioral Findings

We examined the association between the newly-developed CSST and other tasks from our experimental protocol (Fig. 1*b*, Supplemental Table 1). We excluded scores obtained on easy conditions across all difficulty-modulated tasks to prevent ceiling effects, as our cohort composed of high functioning healthy adults (18.13 ± 4.26 years of education; 47 currently employed/studying). Our participants indeed performed close to ceiling for the easy condition (CSST-E), but not the difficult condition (CSST-D) ($t = 16.8$, $P < 0.001$; Supplemental Fig. 1). Furthermore, no sex differences were observed in CSST-D scores (Supplemental Fig. 2). To ensure that the CSST is sensitive to spatial processing, we first cross-referenced it against the well-established FMT paradigm that was administered outside the scanner (Hartley et al. 2007). FMT scores correlated strongly with performances in both the CSST-E ($r = 0.419$, $P = 0.003$; Supplemental Fig. 3) and the CSST-D ($r = 0.406$, $P = 0.004$; Supplemental Fig. 3). Intra-CSST association was also significant ($r = 0.386$; $P = 0.007$; Supplemental Fig. 3). CSST-D and FMT correlations were reproduced when analyzing women and men separately (Supplemental Fig. 4).

Several analyses supported specificity of CSST-D to spatial processing while also noting overlap with relational memory more generally (Fig. 1*b*). Specifically, CSST-D correlated with Sem-D ($r = 0.340$; $P = 0.018$) while showing neither an association with MST ($r = 0.150$; $P = 0.308$) nor with Epi-D ($r = 0.083$; $P = 0.574$). CSST-D also correlated with Sem-E ($r = 0.301$; $P = 0.038$), but not with Epi-E ($r = 0.205$, $P = 0.161$; Supplemental Fig. 3). As expected, CSST-D showed no meaningful associations with MST, Epi-D, and Epi-E when analyzing women and men separately, but

only in men did CSST-D significantly correlate with Sem-D (Supplemental Fig. 4).

### Structural Substrates of Spatial Memory Performance in Neocortical Regions

Controlling for age and sex, we observed positive correlations between CSST-D scores and thickness of bilateral superior temporal, left temporo-polar, bilateral parahippocampal, and left posterior cingulate cortices (Fig. 2a, see Supplemental Fig. 5 for right-handed participants only). Following correction for multiple comparisons ($p_{FWE} < 0.05$), findings were significant in the left superior temporal sulcus ($r = 0.597$), left anteromedial superior temporal gyrus ($r = 0.609$), right posterior parahippocampal gyrus ($r = 0.610$), and the left inferior temporo-occipital junction ($r = 0.591$; Fig. 2b). CSST-D associations were consistent across clusters when separately analyzing both biological sexes (r-values women/men; cluster 1: 0.59/0.62; cluster 2: 0.41/0.72; cluster 3: 0.66/0.62; cluster 4: 0.62/0.63; Supplemental Fig. 6). Notably, average thickness of these four clusters also positively correlated with performance on the FMT ($r = 0.353$; $P = 0.014$; Fig. 2c) and Sem-D ($r = 0.373$; $P = 0.009$; Fig. 2c). Cluster-wise associations ranged between $r = 0.233$–$0.326$ for FMT, and between $r = 0.217$–$0.369$ for Sem-D (Supplemental Fig. 7). Although surface-based associations between thickness and FMT were not significant after multiple comparisons correction, effect size maps were significantly similar to those from the correlation between thickness and CSST-D after correction for age and sex ($r = 0.472$, nonparametric $P < 0.001$: Alexander-Bloch et al. 2018) (Supplemental Fig. 8). Cortical thickness did not correlate with scores in other tasks for the same significance criteria, indicating specificity of the observed brain-behavior correlations. These findings implicate local regions within the left temporal lobe as well as the right MTL as cortical substrates underlying interindividual differences in aptitude on the CSST-D.

### Structural Substrates of Spatial Memory Performance in Hippocampal Subregions

Controlling for effects of age and sex, we observed a trend between CSST-D scores and total hippocampal volume ($r = 0.234$, one-tailed $P = 0.052$). While no surface-wide association passed stringent criteria for multiple comparisons corrections (i.e., $p_{FWE} < 0.05$; CDT = 0.001), we observed uncorrected associations between CSST-D and hippocampal columnar volumes along the long axis of each subfield (Supplemental Fig. 9).

### Functional Contextualization

We contextualized the structural imaging findings with respect to areas relevant for spatial cognition, using task-based fMRI activation maps obtained from the same participants and Neurosynth-based meta-analysis. We contrasted estimated parameters for retrieval and encoding within each participant to control for visual processes common to both phases for the same trial. This subtraction contrast also allowed us to separate the cognitive processes believed to be implicated in CSST performance. Specifically, we expected the retrieval phase to require both successful encoding and successful delayed matching of the given spatial configuration. Thus, contrasting both trial phases can capture neural mechanisms specific to topographical memory recall. We pooled data across CSST-E and CSST-D trials (Supplemental Table 2) as one-tailed *t*-tests failed to ascertain significant group-level activation differences between conditions. We then mapped the volumetric second-level activations (Supplemental Fig. 10, Supplemental Table 3) to fsaverage and computed average cortical thickness in highlighted regions, which showed no correlation with CSST-D scores ($r = 0.189$, one-tailed $P = 0.110$; Fig. 3a, Supplemental Fig. 11a). An additional ad hoc meta-analysis was also performed (Fig. 3b, Supplemental Fig. 11b); here, the Neurosynth-derived map was similarly mapped to fsaverage and average cortical thickness in activated areas was computed. We observed a significant association between CSST-D behavioral performance and average thickness across Neurosynth-derived regions ($r = 0.319$, one-tailed $P = 0.014$).

### Modulatory Effect of Task Performance on Functional Connectivity Profile

We conducted exploratory seed-based connectivity analyses centered on clusters of findings from the structural analyses (i.e., left superior temporal sulcus, left anteromedial superior temporal gyrus, right posterior parahippocampal gyrus, and the left inferior temporo-occipital junction) (Fig. 4). Accounting for age and sex, we observed a marginal association between CSST-D score and the connectivity strength of the right parahippocampal cluster (seed 3; Fig. 4a) and a region encompassed by the left middle frontal and precentral gyri extending medially via the paracentral lobule into the anterior cingulate ($p_{FWE} = 0.052$; outlined cortical surface on third row; Fig. 4b). Here, individuals with higher scores on CSST-D presented with higher functional connectivity between these nodes. We also found that CSST-D performance positively modulated connectivity between the left superior temporal sulcus (seed 1; Fig. 4a) and left CA1–3 ($p_{FWE} = 0.014$; outlined hippocampal surface on first row; Fig. 4b). A similar modulation was seen for the cluster in the left inferior temporo-occipital junction (seed 4; Fig. 4a), which showed connectivity modulation to right CA1–3 by CSST-D ($p_{FWE} = 0.036$; outlined hippocampal surface on fourth row; Fig. 4b).

## Discussion

Our goal was to design a novel cognitive task to evaluate the ability to encode and retrieve spatial relationships between unrelated objects in humans and to identify the neural substrates of such spatial processing via structural and functional connectivity analyses. To this end, we developed and administered the new CSST to 48 healthy young adults as part of a larger task-based fMRI battery and conducted structural and resting-state fMRI (rs-fMRI) analyses. In addition to the CSST, our battery also included a semantic association task and an episodic memory task that were developed in concert with the CSST to address questions pertaining to relational memory more generally. All three tasks were homogenized in terms of visual stimuli, task difficulty and duration, as well as in terms of response paradigm (i.e., three-alternative forced choice). These tests were further optimized for administration outside as well as inside the scanner and are made openly available. An additional test for assessing mnemonic discrimination was also included. Behavioral correlations with additional memory metrics supported relative sensitivity and specificity of the CSST to spatial memory, and some overlap with relational memory more generally. Studying in vivo measures of cortical morphology, we identified substrates underlying interindividual differences in

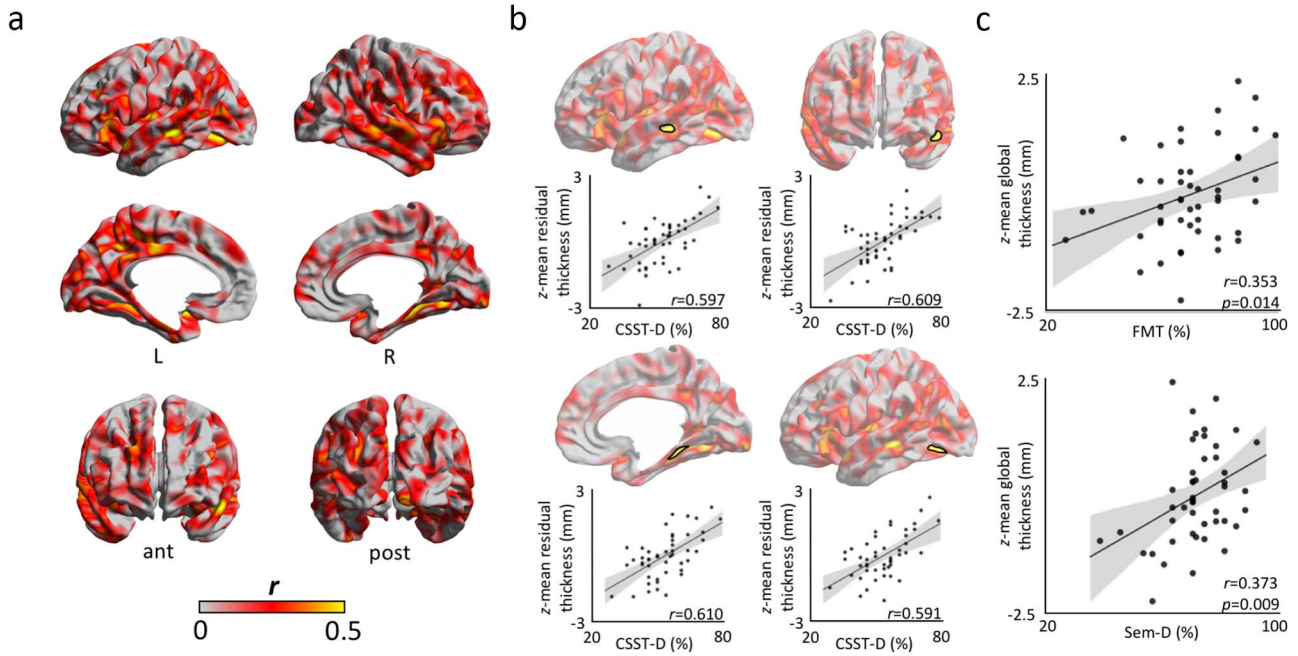


Figure 2. Cortical substrates of the CSST. (*a*) Product–moment correlation coefficients of CSST-D performance on cortical thickness after regressing out age and sex. (*b*) Findings corrected for multiple comparisons ($p_{FWE} < 0.05$; cluster-defining threshold of CDT = 0.001) highlight clusters in the left superior temporal sulcus, left anteromedial superior temporal gyrus, right posterior parahippocampal gyrus, and left inferior temporo-occipital junction. (*c*) Correcting for age and sex, average cortical thickness across clusters of finding showed robust correlations with performance on FMT ($r = 0.353$; $P = 0.014$) and Sem-D ($r = 0.373$; $P = 0.009$).

CSST performance comprising a network of lateral and medial temporal lobe regions. Complementary explorations of rs-fMRI data indicated a stronger functional connectivity of these areas in individuals with higher scores on the CSST. Structural MRI findings could be functionally contextualized by showing overlaps to task-based fMRI activations from the CSST paradigm itself as well as ad hoc meta-analysis. In this work, we present a new paradigm that taps into spatial memory processing, and our multimodal MRI results offer new insights into integrated structure–function substrates of human spatial cognition.

The CSST is an openly accessible (https://github.com/MICA-MNI/micaopen) and convenient python-based protocol that can be administered inside or outside the scanner in less than 15 min. It implements symbolic stimuli in a three-alternative-forced-choice paradigm and consists of two experimental conditions modulated for difficulty (easy: CSST-E; difficult: CSST-D), which is suitable for the study of interindividual variations and between-group differences in the context of healthy and clinical cohorts. The CSST encompasses 56 pseudo-randomized trials (28 per condition) with four equivalent iterations, which can be leveraged to perform multiple probes while controlling for habituation. In addition to paradigm development, we assessed behavioral associations between CSST performance to measures obtained from tasks tapping into spatial, semantic, and episodic dimensions of memory. As this study analyzed high functioning healthy adults, we restricted the analyses to scores obtained on the difficult condition, CSST-D. The CSST-E scores, where our healthy individuals perform close to ceiling, may be more suitable for phenotyping individuals with deficits in spatial cognition, including older adults (Perlmutter et al. 1981; Pezdek 1983; Bohbot et al. 2012) and those with neurological disorders (Bird et al. 2010). In our cohort, CSST-D results correlated with FMT scores measured outside the scanner, suggesting that the task is sensitive to topographic memory. Interestingly, behavioral outcome on the CSST-D was neither correlated with scores on an episodic paired-associates task nor with performance on a mnemonic discrimination task. However, we did observe a correlation with a semantic decision-making task, and in a prior study we had also found that the spatial and semantic aspects of memory were associated via the organization of connectivity between the hippocampus and the lateral temporo-parietal cortex (Sormaz et al. 2017).

Following these behavioral explorations, we utilized the CSST to determine potential structural correlates of interindividual differences in spatial cognition. We examined whether interindividual differences in CSST-D scores correlated to MRI-derived neocortical thickness and hippocampal columnar volume measures. Accounting for variance explained by age and sex, we observed associations with the thickness of bilateral superior temporal, left temporo-polar, bilateral parahippocampal, and left posterior cingulate areas. Following multiple comparisons correction, findings clustered within left lateral temporal and right medial temporal lobe areas, notably the right posterior parahippocampus. As a primary relay between the allo-cortical subregions of the hippocampal formation and the isocortex, the parahippocampal cortex plays an essential role in different forms of spatial processing, including memory for scenes and configuration of objects (Aguirre et al. 1996; Bohbot et al. 1998; Epstein and Kanwisher 1998; Abrahams et al. 1999; Bohbot et al. 2000; Bohbot et al. 2015). Increased gray matter volume of the entorhinal cortex has previously been associated with improved performance on games that rely on geometric relationships, such as Tetris and Minesweeper, as well as platform games, such as Super Mario 64 (Kühn and Gallinat 2014). One study also found an increase in gray matter thickness of bilateral parahippocampal cortex

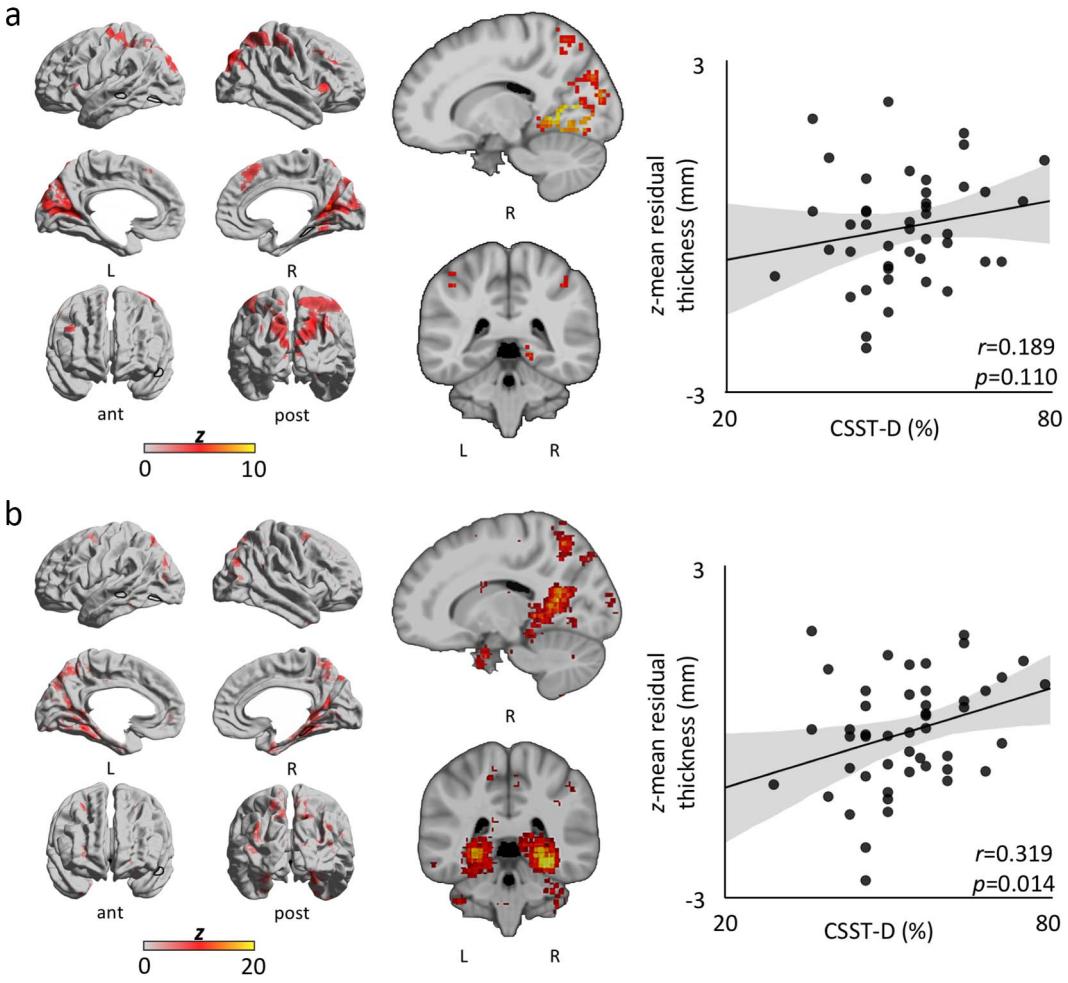


Figure 3. Functional contextualization. To further address task validity, CSST-D scores were correlated with average cortical thickness across regions of activation from CSST- and Neurosynth-derived maps. (*a*) Left column: Group level (n = 44) CSST surface-wide activation for "retrieval-versus-encoding" weighted contrast. Notably, the right PHG shows significant activation. Dark outlines correspond to structural clusters. Middle column: volumetric activation (MNI coordinates: 15, −40). Right column: Trend between average cortical thickness across regions of activation and CSST-D score ($r = 0.189$, one-tailed $P = 0.110$). (*b*) Left column: Neurosynth-derived surface-wide coactivations for the term "navigation." Dark outlines correspond to structural clusters. Middle column: volumetric activation (MNI coordinates: 15, −40). Right column: Significant association between average cortical thickness across coactivated areas and CSST-D performance ($r = 0.319$, one-tailed $P = 0.014$).

following 15 daily gaming sessions on a first-person shooter platform, with long-lasting changes in the left parahippocampal cortex (Momi et al. 2018). The authors argued that detailed environmental mapping of the virtual arena conferred a competitive advantage as evidenced by continued navigation during episodes of virtual blindness (i.e., when hit by smoke or flashbang grenades). However, too great a reliance on the response strategy mediated by the caudate nucleus, which is the most favored spontaneous navigational behavior in first-person shooter paradigms, has instead been shown to shrink the hippocampus (West et al. 2018). Functional neuroimaging paradigms have further implicated the parahippocampal gyrus in object-location retrieval (Owen et al. 1996), local geometry encoding (Epstein and Kanwisher 1998; Epstein 2008), fine-grained spatial judgment (Hirshhorn et al. 2012), and 3D space representation (Kim and Maguire 2018). In line with previous findings, our observations suggest that measures of parahippocampal gray matter could serve as a proxy for cortico-hippocampal information coherence, with greater efficiency of the system translating into better spatial cognition skills. Although their core microstructural changes are incompletely understood, it has been suggested that variations in cortical thickness may, nonetheless, capture underlying variations in cytoarchitecture. For example, while thickness measurements may be anti-correlated to neuronal density, regions of relatively high thickness with reduced density may instead present with more complex dendritic arborization, which could facilitate integrative information processing (Collins et al. 2010; la Fougère et al. 2011; Cahalane et al. 2012; Wagstyl et al. 2015).

Regarding the hippocampus, we observed a positive trend between CSST-D scores and total hippocampal volume. The hippocampus has long been associated with spatial processing in experimental work in animals (O'Keefe and Nadel 1978; Aggleton et al. 1986; Sargolini et al. 2006; Burgess et al. 2007), as well as in lesional patients (Milner 1965; Smith and Milner 1981; Smith and Milner 1989; Rains and Milner 1994) and human neuroimaging studies (Aguirre et al. 1996; Ghaem et al. 1997; Maguire et al. 1998; Abrahams et al. 1999; Maguire et al. 2000; Hassabis et al. 2009; Robin et al. 2018; Kim and Maguire 2018). Furthermore, task-based fMRI analysis of the CSST paradigm

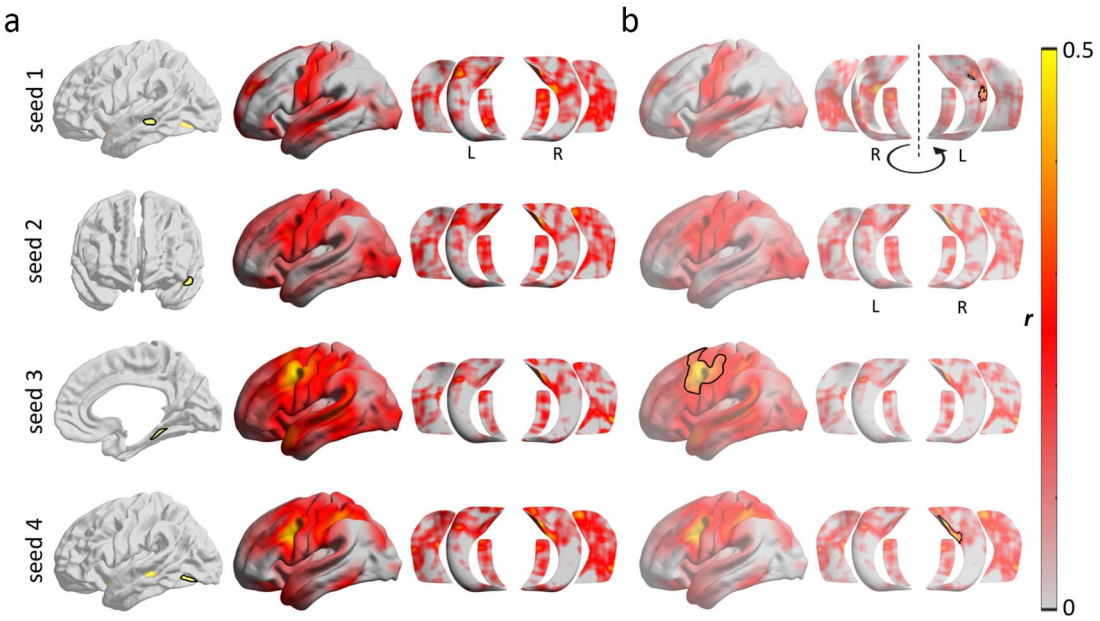


Figure 4. Seed-based resting-state functional connectivity analysis. Analyses focused on clusters of significant structural modulations (see Fig. 2; presented in rows). (*a*) Left column: seeds; Middle and right columns: whole-brain and hippocampal functional connectivity for each seed. (*b*) Associations between CSST-D and connectivity profiles.

and ad hoc meta-analysis via Neurosynth confirmed consistent activations in the hippocampus-parahippocampus complex, particularly in its posterior divisions. It is worth noting that while our result pertaining to the whole hippocampal volume corroborates prior evidence, our analytical approach may not have been sensitive enough to identify subregional effects. Further analyses with larger cohorts and/or higher resolution imaging of the hippocampus are required to more robustly explore subregional substrates in the hippocampus; such approaches may benefit from methodologies that tap into hippocampal longitudinal and medio-lateral axes (Vos de Wael et al. 2018; Plachti et al. 2019; Przeździk et al. 2019; Paquola et al. 2020). Our choice of task-related functional contrasts was informed by the overlap between whole-brain findings for the retrieval-versus-encoding comparison and Neurosynth-based meta-analytical results obtained for the term "navigation". Other contrasts (i.e., easy-vs.-difficult and successful-vs.-unsuccessful trials) failed to yield voxel-wise findings after correction for multiple comparisons. These negative observations mandate in-depth analyses using multivariate approaches in addition to classical univariate methodologies, especially when investigating associations between interindividual variations in functional activation and behavioral outcome measures on the CSST. We will address these questions and more in follow-up studies.

In addition to results pertaining to the MTL, we observed structural MRI effects in lateral temporal areas whose role is less well defined in spatial cognition. Within-sample fMRI and ad hoc meta-analysis results did not support any functional relevance of lateral temporal regions to spatial memory processing and navigation. Several studies have already pointed to contributions from extra-MTL structures such as the posterior cingulate, retrosplenial, dorsolateral prefrontal, and posterior parietal cortices (Aguirre et al. 1996; Ghaem et al. 1997; Maguire et al. 1998; Byrne et al. 2007; Whitlock et al. 2008), but none explicitly to lateral temporal areas. In one virtual-reality fMRI study in which participants navigated a circular platform, grid-cell firing patterns were consistently observed in the lateral temporal cortices, in addition to MTL findings (Doeller et al. 2010). Another experiment showed that movement-onset periods in a square virtual environment were linked to increases in theta frequency power mainly within the hippocampus, but also across the lateral temporal lobes, with greater changes in theta power for relatively longer path lengths (Bush et al. 2017). A meta-analytic review also found that bilateral lateral temporal cortices participated in the processing of familiar as opposed to recently learned virtual environments (Boccia et al. 2014). Interestingly, the same review also reported greater involvement of the right parahippocampus in recently learned virtual settings when compared with familiar ones. Our observation that measurements of cortical thickness across disparate clusters within the left lateral temporal lobe correlate with performance on the CSST-D corroborates previous findings regarding a complementary role of lateral temporal areas to medial regions in spatial processing.

To provide network-level context for these structural findings, we implemented seed-based rs-fMRI connectivity analyses centered on lateral and medial temporal clusters where morphological associations to CSST-D performance were seen. Using more exploratory thresholding, we observed a positive association between CSST-D scores and the connectivity strength between components of this network, specifically between medial and lateral temporal regions, together with a region denoted laterally by the middle frontal and precentral gyri, and medially by the paracentral lobule and superior anterior cingulate. Significant connectivity modulations were obtained for three out of four clusters that showed main effects of CSST-D on cortical thickness; such a combined effect on morphology and functional connectivity speaks to intracortical and network level substrates underlying spatial cognition. Since the discovery of rodent place cells (O'Keefe and Dostrovsky 1971)

and the formulation of the cognitive map theory (O'Keefe and Nadel 1978), which primarily focused on the hippocampus, the neural landscape of spatial cognition has increasingly been conceptualized as a network that encompasses widespread brain areas that perform complementary operations. One leading model posits a vast circuit involving MTL and extra-MTL regions that participate in the reciprocal transformation of body-centered and subject-invariant spatial representations (Byrne et al. 2007; Dhindsa et al. 2014; Bicanski and Burgess 2018). An at times overlooked assumption is that regions involved in specific neural processes may be recruited in various other cognitive domains. Given that the human brain is a finite organ capable of multiple mental functions, it is not surprising that many neural operations show anatomical convergence. In fact, some of the regions discussed herein in the context of spatial memory may apply equally as well to other related cognitive faculties (Constantinescu et al. 2016; Epstein et al. 2017; Bellmund et al. 2018; Mok and Love 2019).

Thus, the behavioral correlation that we observed between spatial and semantic memory scores could point to shared mechanisms across different mnemonic domains. This finding is in line with prior literature suggesting such functional versatility of the hippocampus, which is likely predicated on its structural connectivity to other brain systems (Nadel and Moscovitch 1997; Moscovitch et al. 2005). Notably, associations between semantic and spatial processing also paralleled our recent study of individual differences in different types of memory (Sormaz et al. 2017). In this study, we found that both semantic and spatial memory were related through their association between hippocampal and lateral parietal connectivity at rest. It has been proposed that the brain may organize semantic information as a navigable conceptual mental space, a mechanism not unlike the encoding of spatial information into a cognitive map via the consorted activity of hippocampal place cells and entorhinal grid cells (O'Keefe and Dostrovsky 1971; Hafting et al. 2005; McNaughton et al. 2006; Constantinescu et al. 2016). New evidence further indicates that these cell populations are in fact functionally more flexible than previously believed. For example, it has been argued that the neural mechanisms that encode for Euclidean space may also eventuate a multitude of orthogonally stable cognitive spaces, each representing a unique dimension of experience, such as conceptual knowledge (Bellmund et al. 2018). Recent findings support the involvement of domain-invariant learning algorithms that apply to the neural organization of both spatial and semantic information (Mok and Love 2019). By implementing our newly developed CSST in conjunction with stimulus-matched episodic and semantic memory paradigms, it may be possible to efficiently explore the degree of structural and functional convergence across relational memory domains both in healthy as well diseased populations.

## Supplementary Material

Supplementary material can be found at *Cerebral Cortex* online.

## Funding

Faculty of Medicine studentship from McGill University (to S.T.); China Scholarship Council (CSC) (to Q.L.); fellowship from the Canadian Open Neuroscience Platform (CONP) and CIHR (to J.R.); studentships from the Savoy foundation for Epilepsy and the Richard and Ann Sievers award (to R.V.d.W.); Canadian Institutes of Health Research (CIHR) (to S.L.); postdoctoral fellowship of the Fonds de la Recherche du Quebec—Santé (FRQ-S) (to C.P.); European Research Council (Project ID: 771863—FLEXSEM to E.J.); FRQ-S and CIHR (MOP-57840, MOP-123520 to A.B. and N.B.); European Research Council (WANDERINGMINDS-ERC646927 to J.S.); CIHR (Grant Number 274766 to V.B.); PhD Scholarship from Brain Research UK (award 14181) to L.C.; Berkeley Fellowship (UCL and Gonville and Caius College, Cambridge to L.C.); National Science and Engineering Research Council of Canada (NSERC Discovery-1304413 to B.B.); Canadian Institutes of Health Research (CIHR FDN-154298 to B.B.); SickKids Foundation (NI17–039 to B.B.), Azrieli Center for Autism Research (ACAR-TACC to B.B.); BrainCanada (to B.B.); Tier-2 Canada Research Chairs program (to B.B.).

## Notes

The authors would like to express their gratitude to the MRI technicians at the Montreal Neurological Institute.

## References

Abrahams S, Morris RG, Polkey CE, Jarosz JM, Cox TC, Graves M, Pickering A. 1999. Hippocampal involvement in spatial and working memory: a structural MRI analysis of patients with unilateral mesial temporal lobe sclerosis. *Brain Cogn*. 41(1):39–65.

Aggleton JP, Hunt PR, Rawlins JNP. 1986. The effects of hippocampal lesions upon spatial and non-spatial tests of working memory. *Behav Brain Res*. 19(2):133–146.

Aguirre GK, D'Esposito M. 1997. Environmental knowledge is subserved by separable dorsal/ventral neural areas. *J Neurosci*. 17(7):2512–2518.

Aguirre GK, Detre JA, Alsop DC, D'Esposito M. 1996. The parahippocampus subserves topographical learning in man. *Cereb Cortex*. 6(6):823–829.

Alexander-Bloch AF, Shou H, Liu S, Satterthwaite TD, Glahn DC, Shinohara RT, Vandekar SN, Raznahan A. 2018. On testing for spatial correspondence between maps of human brain structure and function. *Neuroimage*. 178:540–551.

Bellmund JLS, Gärdenfors P, Moser EI, Doeller CF. 2018. Navigating cognition: spatial codes for human thinking. *Science*. 362(6415): eaat6766.

Bernhardt BC, Bernasconi A, Liu M, Hong S-J, Caldairou B, Goubran M, Guiot MC, Hall J, Bernasconi N. 2016. The spectrum of structural and functional imaging abnormalities in temporal lobe epilepsy. *Ann Neurol*. 80(1):142–153.

Bicanski A, Burgess N. 2018. A neural-level model of spatial memory and imagery. *Elife*. 7. doi: 10.7554/eLife.33752.

Bird CM, Chan D, Hartley T, Pijnenburg YA, Rossor MN, Burgess N. 2010. Topographical short-term memory differentiates Alzheimer's disease from frontotemporal lobar degeneration. *Hippocampus*. 20(10):1154–1169.

Biswal BB, Van Kylen J, Hyde JS. 1997. Simultaneous assessment of flow and BOLD signals in resting-state functional connectivity maps. *NMR Biomed*. 10(4–5):165–170.

Boccia M, Nemmi F, Guariglia C. 2014. Neuropsychology of environmental navigation in humans: review and meta-analysis of FMRI studies in healthy participants. *Neuropsychol Rev*. 24(2):236–251.

Bohbot VD, Allen JJ, Nadel L. 2000. Memory deficits characterized by patterns of lesions to the hippocampus and parahippocampal cortex. *Ann N Y Acad Sci*. 911(1):355–368.

Bohbot VD, Allen JJB, Dagher A, Dumoulin S, Evans AC, Petrides M, Kalina M, Stepankova K, Nadel L. 2015. Role of the parahipppocampal cortex in memory for the configuration but not identity of objects: converging evidence from patients with selective thermal lesions and fMRI. *Front Human Neurosci*. 9(431):1–17.

Bohbot VD, Kalina M, Stepankova K, Spackova N, Petrides M, Nadel L. 1998. Spatial memory deficits in patients with lesions to the right hippocampus and to the right parahippocampal cortex. *Neuropsychologia*. 36(11): 1217–1238.

Bohbot VD, McKenzie S, Konishi K, Fouquet C, Kurdi V, Schachar R, Boivin M, Robaey P. 2012. Virtual navigation strategies from childhood to senescence: evidence for changes across the life span. *Front Aging Neurosci*. 4:28.

Buckner RL, Krienen FM, Yeo BTT. 2013. Opportunities and limitations of intrinsic functional connectivity MRI. *Nat Neurosci*. 16(7):832–837.

Burgess N, Barry C, O'Keefe J. 2007. An oscillatory interference model of grid cell firing. *Hippocampus*. 17(9):801–812.

Bush D, Bisby JA, Bird CM, Gollwitzer S, Rodionov R, Diehl B, McEvoy AW, Walker MC, Burgess N. 2017. Human hippocampal theta power indicates movement onset and distance travelled. *Proc Natl Acad Sci U S A*. 114(46):12297–12302.

Byrne P, Becker S, Burgess N. 2007. Remembering the past and imagining the future: a neural model of spatial memory and imagery. *Psychol Rev*. 114(2):340–375.

Cahalane DJ, Charvet CJ, Finlay BL. 2012. Systematic, balancing gradients in neuron density and number across the primate isocortex. *Front Neuroanat*. 6:28.

Caldairou B, Bernhardt BC, Kulaga-Yoskovitz J, Kim H, Bernasconi N, Bernasconi A. 2016. A surface patch-based segmentation method for hippocampal subfields. In: *Medical Image Computing and Computer-Assisted Intervention—MICCAI 2016*. Cham: Springer International Publishing, pp. 379–387.

Cardinale F, Chinnici G, Bramerio M, Mai R, Sartori I, Cossu M, Lo Russo G, Castana L, Colombo N, Caborni C *et al*. 2014. Validation of FreeSurfer-estimated brain cortical thickness: comparison with histologic measurements. *Neuroinformatics*. 12(4):535–542.

Collins CE, Airey DC, Young NA, Leitch DB, Kaas JH. 2010. Neuron densities vary across and within cortical areas in primates. *Proc Natl Acad Sci U S A*. 107(36):15927–15932.

Constantinescu AO, OReilly JX, Behrens TEJ. 2016. Organizing conceptual knowledge in humans with a gridlike code. *Science*. 352(6292):1464–1468.

Cordes D, Haughton VM, Arfanakis K, Wendt GJ, Turski PA, Moritz CH, Quigley MA, Meyerand ME. 2000. Mapping functionally related regions of brain with functional connectivity MR imaging. *AJNR Am J Neuroradiol*. 21(9):1636–1644.

Cox RW. 1996. AFNI: software for analysis and visualization of functional magnetic resonance neuroimages. *Comput Biomed Res*. 29(3):162–173.

Dale AM, Fischl B, Sereno MI. 1999. Cortical surface-based analysis. I. Segmentation and surface reconstruction. *Neuroimage*. 9(2):179–194.

Dhindsa K, Drobinin V, King J, Hall GB, Burgess N, Becker S. 2014. Examining the role of the temporo-parietal network in memory, imagery, and viewpoint transformations. *Front Hum Neurosci*. 8:709.

Doeller CF, Barry C, Burgess N. 2010. Evidence for grid cells in a human memory network. *Nature*. 463(7281): 657–661.

Ekstrom AD, Kahana MJ, Caplan JB, Fields TA, Isham EA, Newman EL, Fried I. 2003. Cellular networks underlying human spatial navigation. *Nature*. 425(6954):184–188.

Epstein R, Kanwisher N. 1998. A cortical representation of the local visual environment. *Nature*. 392(6676):598–601.

Epstein RA. 2008. Parahippocampal and retrosplenial contributions to human spatial navigation. *Trends Cogn Sci*. 12(10):388–396.

Epstein RA, Patai EZ, Julian JB, Spiers HJ. 2017. The cognitive map in humans: spatial navigation and beyond. *Nat Neurosci*. 20(11):1504–1513.

Fischl B. 2012. FreeSurfer. *Neuroimage*. 62(2):774–781.

Fischl B, Sereno MI, Tootell RB, Dale AM. 1999. High-resolution intersubject averaging and a coordinate system for the cortical surface. *Hum Brain Mapp*. 8(4):272–284.

la Fougère C, Grant S, Kostikov A, Schirrmacher R, Gravel PS, Schipper MH, Reader A, Evans A, Thiel A. 2011. Where in-vivo imaging meets cytoarchitectonics: the relationship between cortical thickness and neuronal density measured with high-resolution [18F]flumazenil-PET. *NeuroImage*. 56(3): 951–960.

Fox MD, Corbetta M, Snyder AZ, Vincent JL, Raichle ME. 2006. Spontaneous neuronal activity distinguishes human dorsal and ventral attention systems. *Proc Natl Acad Sci U S A*. 103(26):10046–10051.

Ghaem O, Mellet E, Crivello F, Tzourio N, Mazoyer B, Berthoz A, Denis M. 1997. Mental navigation along memorized routes activates the hippocampus, precuneus, and insula. *Neuroreport*. 8(3):739–744.

Goubran M, Ntiri EE, Akhavein H, Holmes M, Nestor S, Ramirez J, Adamo S, Ozzoude M, Scott C, Gao F *et al*. 2020. Hippocampal segmentation for brains with extensive atrophy using three-dimensional convolutional neural networks. *Hum Brain Mapp*. 41(2):291–308.

Greve DN, Fischl B. 2009. Accurate and robust brain image alignment using boundary-based registration. *Neuroimage*. 48(1):63–72.

Hafting T, Fyhn M, Molden S, Moser M-B, Moser EI. 2005. Microstructure of a spatial map in the entorhinal cortex. *Nature*. 436(7052):801–806.

Han L, Kashyap AL, Finin T, Mayfield J, Weese J. 2013. *UMBC_EBIQUITY-CORE: Semantic Textual Similarity Systems*. Atlanta: Association for Computational Linguistics, pp. 44–52.

Hartley T, Bird CM, Chan D, Cipolotti L, Husain M, Vargha-Khadem F, Burgess N. 2007. The hippocampus is required for short-term topographical memory in humans. *Hippocampus*. 17(1):34–48.

Hartley T, Harlow R. 2012. An association between human hippocampal volume and topographical memory in healthy young adults. *Front Hum Neurosci*. 6:338.

Hassabis D, Chu C, Rees G, Weiskopf N, Molyneux PD, Maguire EA. 2009. Decoding neuronal ensembles in the human hippocampus. *Curr Biol*. 19(7):546–554.

He T, Kong R, Holmes AJ, Nguyen M, Sabuncu MR, Eickhoff SB, Bzdok D, Feng J, Yeo BTT. 2020. Deep neural networks and kernel regression achieve comparable accuracies for functional connectivity prediction of behavior and demographics. *Neuroimage*. 206(116276):116276.

Hirshhorn M, Grady C, Rosenbaum RS, Winocur G, Moscovitch M. 2012. Brain regions involved in the retrieval of spatial and

episodic details associated with a familiar environment: an fMRI study. *Neuropsychologia*. 50(13):3094–3106.
Jacobs J, Weidemann CT, Miller JF, Solway A, Burke JF, Wei X-X, Suthana N, Sperling MR, Sharan AD, Fried I *et al*. 2013. Direct recordings of grid-like neuronal activity in human spatial navigation. *Nat Neurosci*. 16(9):1188–1190.
Jenkinson M, Beckmann CF, Behrens TEJ, Woolrich MW, Smith SM. 2012. FSL. *Neuroimage*. 62(2):782–790.
Jokeit H, Okujava M, Woermann FG. 2001. Memory fMRI lateralizes temporal lobe epilepsy. *Neurology*. 57(10):1786–1793.
Kim H, Bernhardt BC, Kulaga-Yoskovitz J, Caldairou B, Bernasconi A, Bernasconi N. 2014. Multivariate hippocampal subfield analysis of local MRI intensity and volume: application to temporal lobe epilepsy. *Med Image Comput Comput Assist Interv*. 17(Pt 2):170–178.
Kim JS, Singh V, Lee JK, Lerch J, Ad-Dab'bagh Y, MacDonald D, Lee JM, Kim SI, Evans AC. 2005. Automated 3-D extraction and evaluation of the inner and outer cortical surfaces using a Laplacian map and partial volume effect classification. *Neuroimage*. 27(1):210–221.
Kim M, Maguire EA. 2018. Hippocampus, retrosplenial and parahippocampal cortices encode multicompartment 3D space in a hierarchical manner. *Cereb Cortex*. 28(5): 1898–1909.
Kühn S, Gallinat J. 2014. Amount of lifetime video gaming is positively associated with entorhinal, hippocampal, and occipital volume. *Molecular Psychiatry*. 19:842–847.
Kulaga-Yoskovitz J, Bernhardt BC, Hong S-J, Mansi T, Liang KE, van der Kouwe AJW, Smallwood J, Bernasconi A, Bernasconi N. 2015. Multi-contrast submillimetric 3 tesla hippocampal subfield segmentation protocol and dataset. *Sci Data*. 2(1):150059.
Kuperberg GR, Broome MR, McGuire PK, David AS, Eddy M, Ozawa F, Goff D, West WC, Williams SCR, van der Kouwe AJW *et al*. 2003. Regionally localized thinning of the cerebral cortex in schizophrenia. *Arch Gen Psychiatry*. 60(9):878–888.
Lowe MJ, Dzemidzic M, Lurito JT, Mathews VP, Phillips MD. 2000. Correlations in low-frequency BOLD fluctuations reflect cortico-cortical connections. *Neuroimage*. 12(5):582–587.
Maguire EA, Burgess N, Donnett JG, Frackowiak RS, Frith CD, O'Keefe J. 1998. Knowing where and getting there: a human navigation network. *Science*. 280(5365):921–924.
Maguire EA, Gadian DG, Johnsrude IS, Good CD, Ashburner J, Frackowiak RS, Frith CD. 2000. Navigation-related structural change in the hippocampi of taxi drivers. *Proc Natl Acad Sci U S A*. 97(8):4398–4403.
McNaughton BL, Battaglia FP, Jensen O, Moser EI, Moser M-B. 2006. Path integration and the neural basis of the "cognitive map.". *Nat Rev Neurosci*. 7(8):663–678.
Medea B, Karapanagiotidis T, Konishi M, Ottaviani C, Margulies D, Bernasconi A, Bernasconi N, Bernhardt BC, Jefferies E, Smallwood J. 2018. How do we decide what to do? Resting-state connectivity patterns and components of self-generated thought linked to the development of more concrete personal goals. *Exp Brain Res*. 236(9):2469–2481.
Milner B. 1965. Visually-guided maze learning in ma: effects of bilateral hippocampal, bilateral frontal, and unilateral cerebral lesions. *Neuropsychologia*. 3(4):317–338.
Mok RM, Love BC. 2019. A non-spatial account of place and grid cells based on clustering models of concept learning. *Nat Commun*. 10(1):5685.
Momi D, Smeralda C, Sprugnoli G, Ferrone S, Rossi S, Rossi A, Di Lorenzo G, Santarnecchi E. 2018. Acute and long-lasting cortical thickness changes following intensive first-person action videogame practice. *Behav Brain Res*. 353:62–73.
Morris RG, Garrud P, Rawlins JN, O'Keefe J. 1982. Place navigation impaired in rats with hippocampal lesions. *Nature*. 297(5868):681–683.
Moscovitch M, Rosenbaum RS, Gilboa A, Addis DR, Westmacott R, Grady C, McAndrews MP, Levine B, Black S, Winocur G *et al*. 2005. Functional neuroanatomy of remote episodic, semantic, and spatial memory: a unified account based on multiple trace theory. *J Anatomy*. 207(1):35–66.
Nadel L, Moscovitch M. 1997. Memory consolidation, retrograde amnesia and the hippocampal complex. *Curr Opin Neurobiol*. 7(2):217–227.
O'Keefe J, Dostrovsky J. 1971. The hippocampus as a spatial map: preliminary evidence from unit activity in the freely-moving rat. *Brain Res*. 34(1):171–175.
O'Keefe J, Nadel L. 1978. *The Hippocampus as a Cognitive Map*. London, England: Oxford University Press.
Owen AM, Milner B, Petrides M, Evans AC. 1996. A specific role for the right parahippocampal gyrus in the retrieval of object-location: a positron emission tomography study. *J Cogn Neurosci*. 8(6):588–602.
Paquola C, Benkarim O, DeKraker J, Larivière S, Frässle S, Royer J, Tavakol S, Valk S, Bernasconi A, Bernasconi N *et al*. 2020. Convergence of cortical types and functional motifs in the human mesiotemporal lobe. *Elife*. 9. doi: 10.7554/eLife.60673.
Payne JD, Tucker MA, Ellenbogen JM, Wamsley EJ, Walker MP, Schacter DL, Stickgold R. 2012. Memory for semantically related and unrelated declarative information: the benefit of sleep, the cost of wake. *PLoS One*. 7(3): e33079.
Perlmutter M, Metzger R, Nezworski T, Miller K. 1981. Spatial and temporal memory in 20 to 60 year olds. *J Gerontol*. 36(1):59–65.
Pezdek K. 1983. Memory for items and their spatial locations by young and elderly adults. *Dev Psychol*. 19(6):895–900.
Plachti A, Eickhoff SB, Hoffstaedter F, Patil KR, Laird AR, Fox PT, Amunts K, Genon S. 2019. Multimodal parcellations and extensive behavioral profiling tackling the hippocampus gradient. *Cereb Cortex*. 29(11):4595–4612.
Przeździk I, Faber M, Fernández G, Beckmann CF, Haak KV. 2019. The functional organization of the hippocampus along its long-axis is gradual and predicts recollection. *Cortex*. 119:324–335.
Rains GD, Milner B. 1994. Right-hippocampal contralateral-hand effect in the recall of spatial location in the tactual modality. *Neuropsychologia*. 32(10):1233–1242.
Robin J, Buchsbaum BR, Moscovitch M. 2018. The primacy of spatial context in the neural representation of events. *J Neurosci*. 38(11):2755–2765.
Romero JE, Coupé P, Manjón JV. 2017. HIPS: a new hippocampus subfield segmentation method. *Neuroimage*. 163:286–295.
Rosas HD, Liu AK, Hersch S, Glessner M, Ferrante RJ, Salat DH, van der Kouwe A, Jenkins BG, Dale AM, Fischl B. 2002. Regional and progressive thinning of the cortical ribbon in Huntington's disease. *Neurology*. 58(5):695–701.
Sargolini F, Fyhn M, Hafting T, McNaughton BL, Witter MP, Moser M-B, Moser EI. 2006. Conjunctive representation of position, direction, and velocity in entorhinal cortex. *Science*. 312(5774):758–762.
Schindler A, Bartels A. 2013. Parietal cortex codes for egocentric space beyond the field of view. *Curr Biol*. 23(2):177–182.
Smith ML, Milner B. 1981. The role of the right hippocampus in the recall of spatial location. *Neuropsychologia*. 19(6): 781–793.

Smith ML, Milner B. 1989. Right hippocampal impairment in the recall of spatil location: encoding deficit or rapid forgetting. *Neuropsychologia*. 27(1):71–81.

Smith SM, Fox PT, Miller KL, Glahn DC, Fox PM, Mackay CE, Filippini N, Watkins KE, Toro R, Laird AR *et al*. 2009. Correspondence of the brain's functional architecture during activation and rest. *Proc Natl Acad Sci U S A*. 106(31):13040–13045.

Smith SM, Nichols TE, Vidaurre D, Winkler AM, Behrens TEJ, Glasser MF, Ugurbil K, Barch DM, Van Essen DC, Miller KL. 2015. A positive-negative mode of population covariation links brain connectivity, demographics and behavior. *Nat Neurosci*. 18(11):1565–1567.

Sormaz M, Jefferies E, Bernhardt BC, Karapanagiotidis T, Mollo G, Bernasconi N, Bernasconi A, Hartley T, Smallwood J. 2017. Knowing what from where: hippocampal connectivity with temporoparietal cortex at rest is linked to individual differences in semantic and topographic memory. *Neuroimage*. 152:400–410.

Stark SM, Yassa MA, Lacy JW, Stark CEL. 2013. A task to assess behavioral pattern separation (BPS) in humans: data from healthy aging and mild cognitive impairment. *Neuropsychologia*. 51(12):2442–2449.

Styner M, Oguz I, Xu S, Brechbühler C, Pantazis D, Levitt JJ, Shenton ME, Gerig G. 2006. Framework for the statistical shape analysis of brain structures using SPHARM-PDM. *Insight J*. 1071:242–250.

Valk SL, Bernhardt BC, Böckler A, Trautwein F-M, Kanske P, Singer T. 2017. Socio-cognitive phenotypes differentially modulate large-scale structural covariance networks. *Cereb Cortex*. 27(2):1358–1368.

Vos de Wael R, Larivière S, Caldairou B, Hong S-J, Margulies DS, Jefferies E, Bernasconi A, Smallwood J, Bernasconi N, Bernhardt BC. 2018. Anatomical and microstructural determinants of hippocampal subfield functional connectome embedding. *Proc Natl Acad Sci U S A*. 115(40): 10154–10159.

Wagstyl K, Ronan L, Goodyer IM, Fletcher PC. 2015. Cortical thickness gradients in structural hierarchies. *Neuroimage*. 111:241–250.

Wang H, Suh JW, Das SR, Pluta JB, Craige C, Yushkevich PA. 2013. Multi-atlas segmentation with joint label fusion. *IEEE Trans Pattern Anal Mach Intell*. 35(3): 611–623.

Wang X, Bernhardt BC, Karapanagiotidis T, de Caso I, Gonzalez Alam TRDJ, Cotter Z, Smallwood J, Jefferies E. 2018. The structural basis of semantic control: evidence from individual differences in cortical thickness. *Neuroimage*. 181: 480–489.

West GL, Konishi K, Diarra M, Benady-Chorney J, Drisdelle BL, Dahmani L, Sodums DJ, Lepore F, Jolicoeur P, Bohbot VD. 2018. Impact of video games on plasticity of the hippocampus. *Mol Psychiatry*. 23(7):1566–1574.

Whitlock JR, Sutherland RJ, Witter MP, Moser M-B, Moser EI. 2008. Navigating from hippocampus to parietal cortex. *Proc Natl Acad Sci U S A*. 105(39):14755–14762.

Winocur G. 1982. Radial-arm maze behavior by rats with dorsal hippocampal lesions: effects of cuing. *J Comp Physiol Psychol*. 96(2):155–169.

Worsley KJ, Taylor JE, Carbonell F, Chung MK, Duerden E, Bernhardt B, Lyttelton O, Boucher M, Evans AC. 2009. SurfStat: a Matlab toolbox for the statistical analysis of univariate and multivariate surface and volumetric data using linear mixed effects models and random field theory. *Neuroimage*. 47: S102.